24th COBEM - 2017

24th ABCM International Congress of Mechanical Engineering
December 3-8, 2017, Curitiba, PR, Brazil

COBEM-2017-1144
DEVELOPMENT OF PIEZOELECTRIC TRANSDUCERS FOR ACOUSTIC LEVITATION

Igor Martins Genuino
Bruno Eduardo da Costa Lima
Filipe Ieda Fazanaro
Universidade Federal do ABC, Centro de Engenharia, Modelagem e Ciências Sociais Aplicadas, Avenida dos Estados, 5001, Santa Terezinha, 09210-580, Santo André, SP, Brasil
igor.margen@gmail.com, Brunoe.costalima@gmail.com, filipe.fazanaro@ufabc.edu.br

Marco Aurélio Brizzotti Andrade
Instituto de Física, Universidade de São Paulo, Cidade Universitária, 05508-090, Brasil
marcobrizzotti@gmail.com

Abstract. *This work presents the development of Langevin piezoelectric transducers and its application in acoustic levitation of small particles. The transducers consist of two piezoelectric rings sandwiched between aluminum masses by a central bolt. The dynamic behavior of each transducer was simulated by using the Finite Element Method and the transducers were designed to resonate at a frequency of 23 kHz. The Finite Element Method was also applied to simulate the potential of the acoustic radiation force that acts on small particles in a standing wave field. Two transducers were fabricated to experimentally validate the simulation results. The designed and experimental resonance frequencies had relative error smaller than 3%. In addition, the transducers were used to acoustically levitate small expanded polystyrene particles in air.*

Keywords: *Acoustic levitation, Resonance frequency, Standing wave*

1. INTRODUCTION

Contactless manipulation of materials is of great interest in many disciplines, including biology (Scheeline and Behrens, 2012), analytical chemistry (Santesson and Nilsson, 2004), material sciences (Gao *et al.*, 1999) and in microassembly (Vandaele *et al.*, 2005). Although there are different methods to levitate and manipulate materials in a contactless fashion (Brandt, 1989), most of them only work with certain materials. For example, magnetic levitation (Kaplan, 1967) is able to suspend heavy objects, but it is mainly restricted to ferromagnetic materials. Optical levitation (Grier, 2003) has great flexibility, but it can only be applied to relatively transparent microparticles. In contrast, acoustic levitation (Brandt, 2001) can be used with almost any kind of material, including solids (Andrade *et al.*, 2016; Xie *et al.*, 2002), liquids (Yarin *et al.*, 1998), and even small living animals (Xie *et al.*, 2006).

Acoustic levitation is based on the fact that when an object is immersed in an acoustic field, it experiences a force called acoustic radiation force (Bruus, 2012). If the acoustic radiation force is strong enough, it can be used to counteract gravity and suspend small objects in mid-air. For a long time, acoustic levitation was only able to levitate small particles at fixed positions in space, but recent advances in acoustic levitation now allows transporting (Koyama and Nakamura, 2010) and manipulating (Foresti *et al.*, 2013; Marzo *et al.*, 2015) particles in a controllable manner. It has also been demonstrated recently that acoustic levitation can even be applied to levitate objects larger than the acoustic wavelength (Andrade *et al.*, 2016, 2017).

There are different types of acoustic levitators, with the most common being the single-axis device (Andrade *et al.*, 2010; Xie and Wei, 2001). A single-axis acoustic levitator consists of a transducer and a reflector, in which a standing wave is established between them. When small particles are inserted in the levitator, the acoustic radiation force levitates the particles at the pressure nodes of the standing wave. Due to the high acoustic pressure amplitudes required for levitation, acoustic levitators usually operate at ultrasonic frequencies. Although acoustic levitation can be achieved at audible frequencies, the sound pressure level can exceed 160 dB, which can easily lead to hearing loss. For this reason, acoustic levitators are commonly designed to operate at a frequency above 20 kHz.

A typical single-axis acoustic levitator uses a Langevin transducer (Gallego-Juarez, 1989) to produce a ultrasonic standing wave between the transducer radiating face and the reflector. A Langevin transducer consists of pairs of piezoelectric ceramic rings prestressed between two metal masses by a central bolt. This type of transducer has a narrow-band

and its resonance frequency depends on the transducer length, the material properties of the metal masses and the piezoelectric ceramics. Although Langevin transducers are commercially available, many acoustic levitation devices require custom made transducers. Therefore, the transducer design is of great importance in the development of new acoustic levitation devices.

In this context, this work presents the development of 23 kHz Langevin transducers for acoustic levitation. The dynamic behavior of the transducers is simulated by the employment of the Finite Element Method which is also applied to simulate the acoustic pressure distribution between the transducer and a concave reflector. Aiming to experimentally validate the simulation results, two transducers were fabricated and used in the acoustic levitation of small particles in mid-air.

This work is structured as follows: Section 2. describes the transducers development and its corresponding numerical simulations. Section 3. presents the experimental results. In section 4. the conclusions and discussions are presented.

2. TRANSDUCER DESIGN USING THE FINITE ELEMENT METHOD

A typical ultrasonic transducer consists of two main parts: a Langevin actuator and a mechanical amplifier, as illustrated in Figure 1. The Langevin actuator is formed by two piezoelectric rings, which are prestressed between two metal masses by a central bolt. The Langevin actuator is used to convert the electrical energy into mechanical energy. This conversion is achieved by applying alternate electric potentials at the piezoceramics, which, through the piezoelectric effect, cause vibration of the actuator ends. The Langevin actuator is connected to a mechanical amplifier, which has the purpose to amplify the mechanical displacement amplitude.

Each individual transducer part works as a half-wavelength resonator and they should be carefully designed in order to have the same resonance frequency (Silva, 2006). In this context, based on the analysis and discussions provided in (Gallego-Juarez, 1989; Silva, 2006), it was decided to employ two PZT-8 (lead zirconate titanate) ring-shaped piezoelectric ceramics. Together, both ceramics correspond to 11.52% of the transducer body (without considering the amplifier part). The transducer body was constructed using aluminum alloy 7075. The cooper electrodes and the insulation material have, respectively, thickness equal to 0.35 mm and 1 mm.

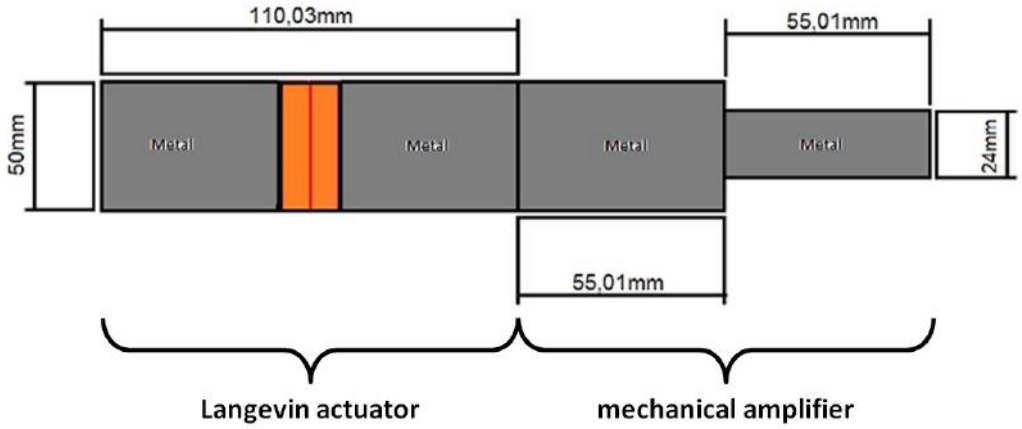

Figure 1: Ultrasonic transducer formed by a Langevin actuator and a mechanical amplifier, with the preliminary transducer dimensions.

2.1 Initial Considerations

As previously specified, two transducers were designed to resonate at a frequency of 23 kHz. Consequently, the length of each transducer part should be equal to a half-wavelength. Therefore, to estimate the initial length of each transducer part, it can be considered that each part consists of a single piece of length L, i.e., in this first step, the piezoceramics and the insulation material can be neglected. Therefore, an initial estimate for the length L can be calculated using (1),

$$L = \frac{c}{2f}, \tag{1}$$

where $f = 23$ kHz and c is the sound velocity through the aluminum. Considering that the Young module (Y) of the aluminum is 74.32 GPa and the density is 2901.30 kg/m^3, employing (2),

$$c = \sqrt{\frac{Y}{\rho}}, \tag{2}$$

one obtains $c = c_A = 5061.24$ m/s. Considering this result in Eq. (1), the length of each transducer part should be equal to 110.03 mm. Therefore, the preliminary dimensions for the transducers were chosen according to the dimensions of Figure 1.

Ideally, a Langevin transducer should vibrate in the longitudinal mode, with minimum coupling with the radial modes. In a transducer with ratio between the diameter and wavelength close to 0.25, practically there is no coupling between longitudinal and radial vibrations. Higher ratios can lead to an overlapping of vibration modes. Therefore, given that the wavelength is equal to $\lambda = 220$ mm and considering a factor of 0.25, the transducer diameter should be less than 55 mm. Therefore, it was chosen a standard diameter equal to 50 mm.

For the smaller diameter face of the transducer amplifier, an amplification ratio close to 4 was desired for the simulations. This relationship is commonly used in early stages of projects similar to the one developed here because, as discussed by Tayra (2014), it already has a great advantage in the overall performance of the transducer without presenting a high risk of damage to the material. Although the higher the amplification ratio, the greater the displacement at the transducer tip, there are limits that the material supports. Therefore, as discussed before, considering that the transducer has a diameter of 50 mm, and aiming that the initial amplification ratio is 4, a value equal to 24 mm was chosen for the smaller diameter face of the amplifier.

From these initial considerations, the COMSOL Multiphysics® finite element software was used to simulate and design the transducers. For each transducer, an iteractive procedure was adopted, where the lengths of each transducer part (i.e. Langevin actuator and mechanical amplifier) were adjusted until the resonance frequency matched the desired frequency of 23 kHz. Figure 2 presents the dimensions, in millimeters, of the designed and constructed transducers.

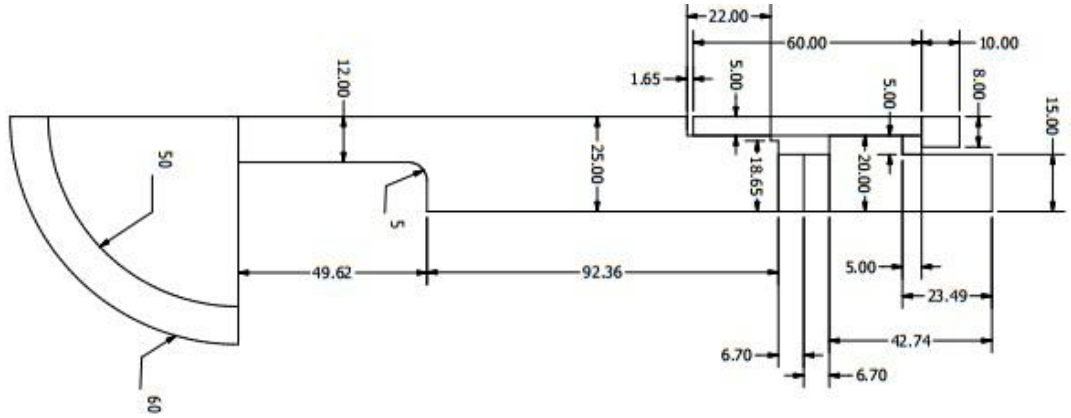

(a) Transducer A.

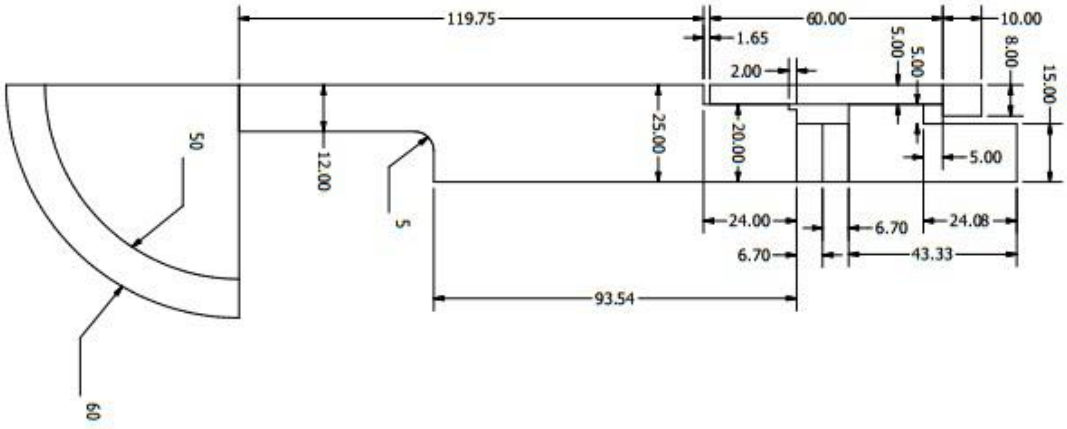

(b) Transducer B.

Figure 2: Transducers developed and simulated using COMSOL Multiphysics®. The units are millimeters.

2.2 Computational Simulations Results

For each transducer design shown in Figure 2, a set of simulations were carried out in the finite element software COMSOL Multiphysics®. The simulation results are presented in the following subsections. Further simulation details can be found in (Lima and Genuino, 2017).

2.2.1 Displacement amplitude of the transducers tip

The displacement amplitude of each transducer tip was simulated as a function of the frequency and it is presented in Figure 3. Figure 3(a) presents the displacement curve for transducer A, showing that the resonance frequency occurs at 23 kHz. According to this curve, the transducer presents a displacement amplitude of 0.007 mm when it is driven at its resonance frequency. The displacement curve for transucer B is presented in Figure 3(b). As expected from the transducer design, transducer B also presents a resonance frequency of 23 kHz, with a displacement amplitude of 0.0019 mm at the resonance.

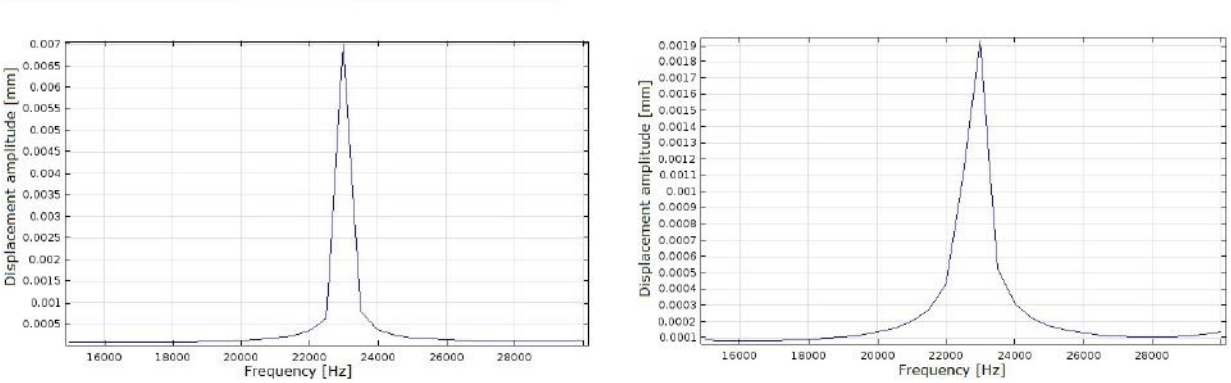

(a) Transducer A. (b) Transducer B.

Figure 3: Simulated displacement amplitude of the transducers tips.

2.2.2 Acoustic pressure

The second set of simulations was performed to verify the maximum total pressure [Pa] generated by transducers in the air at the resonant frequency. For the air simulation, a Perfectly Matched Layer (PML) consisting of a wave layer without reflection was used. The results can be seen in Figure 4 where the color scale varies from red (higher pressure) to blue (lower pressure).

As expected, the pressure is zero in the PML regions, because the function of this region is to absorb the waves. The tip of the transducer slight moves based on the movement of the piezoelectric ceramic. As the ceramic expands in the z-direction, a positive wavefront is generated, which in turn produces a positive pressure and, as it compresses in the z-direction, a negative wavefront is also generated which results in a negative pressure. The acoustic pressure variation of a transducer subjected to the resonant frequency is maximum, because its displacement and energy are maximum, causing, thereby, a greater displacement.

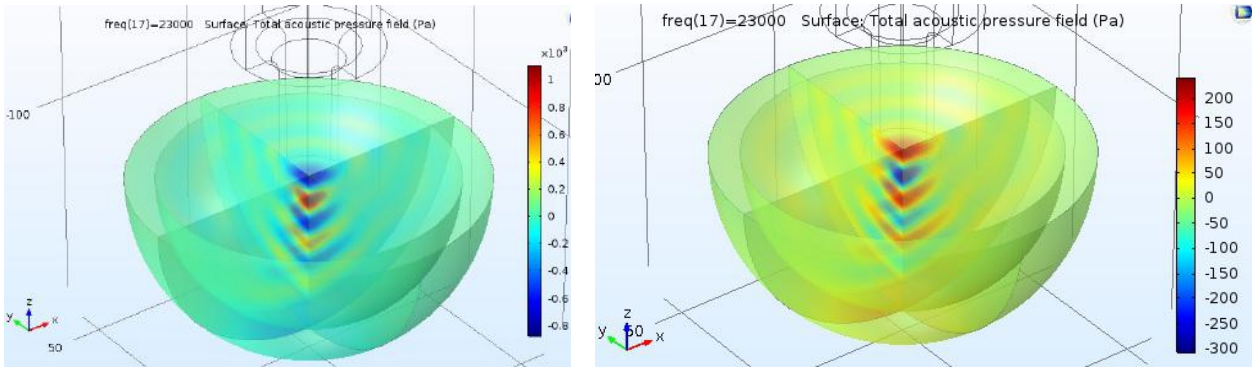

(a) Transducer A. (b) Transducer B.

Figure 4: Acoustic pressure in the air when the transducers are excited at a frequency of 23 kHz.

2.2.3 Analysis of the electric potential related to the piezoelectric ceramics

Figure 5 illustrates the cross-sectional view of the 23-kHz electric potential in the two PZT-8 piezoelectric ceramics. As described in (Lima and Genuino, 2017), the simulation performed in COMSOL Multiphysics® considers that an 80 V is applied to the ceramics of both transducers. Compared to other simulations performed considering different frequencies (22 and 24 kHz; see (Lima and Genuino, 2017, appendix)) for both transducers, it was verified that the electric potential behaves in a "distorted" way. A possible explanation considered here could be associated with the peak of activity and deformation observed at the resonant frequency.

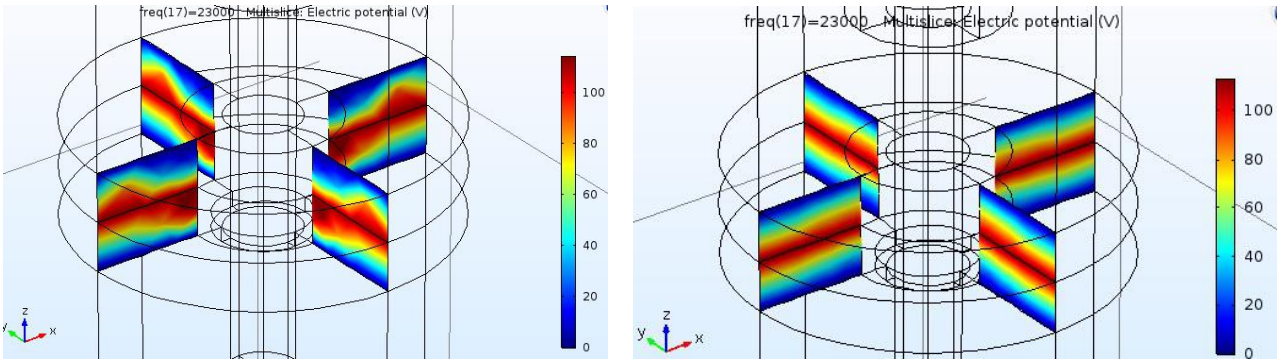

(a) Transducer A. (b) Transducer B.

Figure 5: Electric potential simulated for both PZT-8 piezoelectric ceramics. The color scale indicates the potential values interval.

2.2.4 Mechanical stress

The tensile elasticity is the maximum tension that the material supports within the elastic deformation regime before it begins to experience a definitive deformation. The aeronautical aluminum 7075 used to manufacture the transducers has a high tensile elasticity, of the order of 495 MPa. Figure 6 shows the tension levels in the transducers when operating at the resonant frequency. The maximum tension for transducer A is equal to 20 MPa and for transducer B, 5 MPa. In both cases, these values are obtained in the region of encounter between the largest and the smallest diameters.

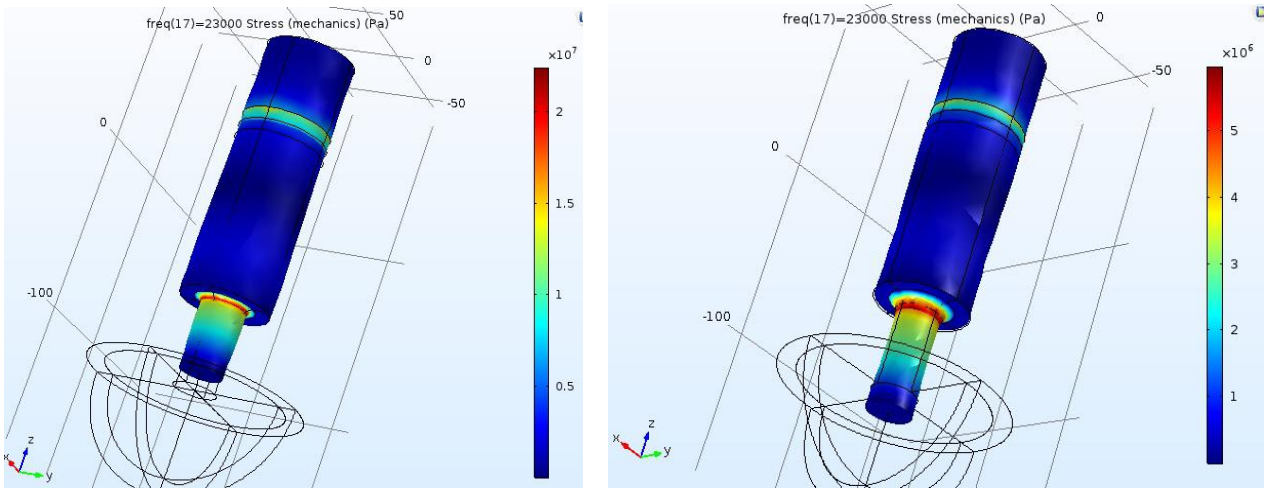

(a) Transducer A. (b) Transducer B.

Figure 6: Tensile elasticity observed for the 23 kHz frequency. Color scale indicates the tension levels observed.

Although the tensions observed in both transducers are much smaller than those supported by aluminum, the results obtained so far prove that the proposed transducers resonate at the desired operating frequency. In addition, the simulated models present structural and electrical characteristics that are feasible for their construction.

2.2.5 Acoustic levitation simulation

The Finite Element Method was also applied to investigate the acoustic levitation of small objects. In this simulation, it was simulated the acoustic pressure distribution between the transducer and a concave reflector. The results presented

in this section were obtained only for transducer A. Further details mainly regarding to the parameters definition of COMSOL Multiphysics® can be obtained in (Lima and Genuino, 2017).

In order to levitate small objects, it is necessary to create a standing wave, which is generated through the multiple wave reflections between the transducer and the reflector located at a distance corresponding to an integer of a half-wavelength from the transducer. The use of a reflector with a concavity is particularly interesting because it increases the axial and lateral forces on the levitated objects, improving its stability (Andrade *et al.*, 2015b). Figure 7 shows the geometry of the reflector. It was also considered that the smaller diameter of the transducers are equal to 24 mm.

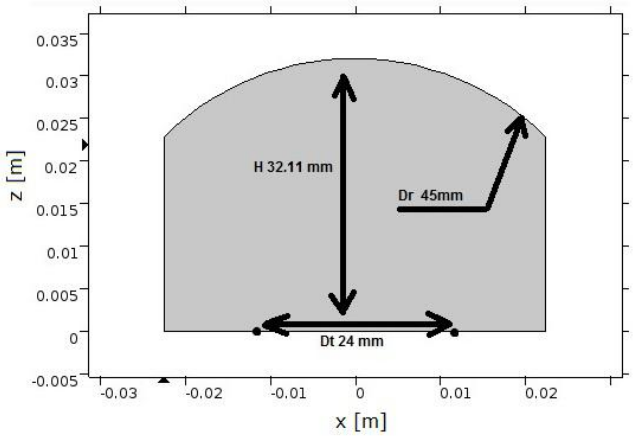

Figure 7: Geometric model of the reflector considered during the experiments.

The main objective of this computational step is to model the air region comprised between the transducer tip and the reflector, defining the transducer and reflector boundaries as the aluminum itself. As discussed by Lima and Genuino (2017, chapter 6), the distance between the extremity of the transducer and the center of the concave reflector was considered to be 32.11 mm. The observed acoustic pressure is illustrated in Figure 8, panel (A), where the color scale indicates the pressure amplitude. It can be observed the existence of a standing wave with node and anti-node regions. The particles are expected to be carried at the equilibrium points (exemplified as black points in the figure), i.e., zero pressure regions between two anti-nodes.

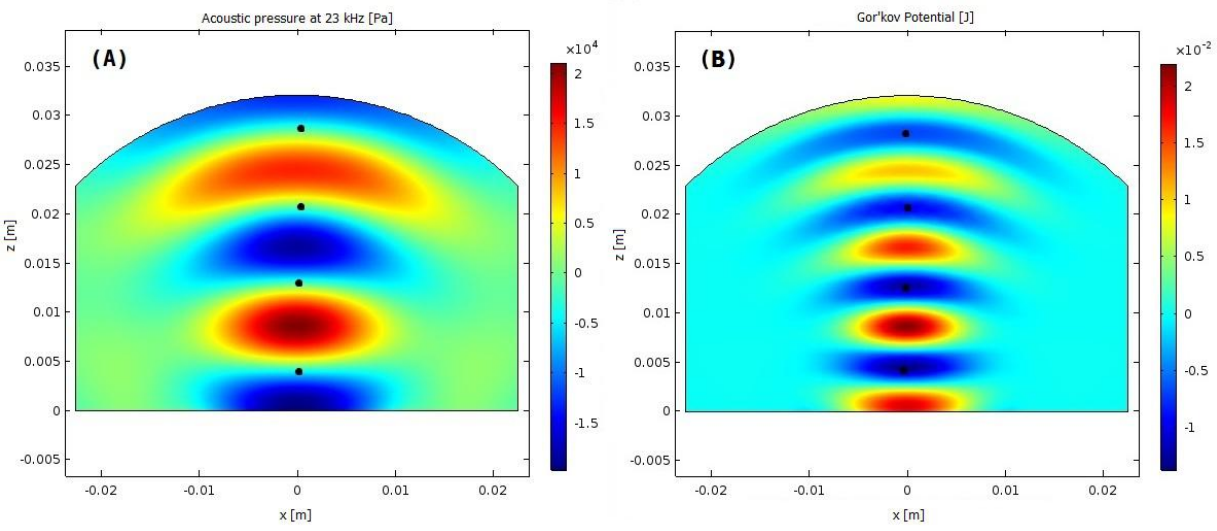

Figure 8: An overview about the expected position of the particle when the levitation occurs. Black dots indicate where the particles will levitate in the air.

The panel (B) of Figure 8 shows the Gor'kov potential [J] which is obtained using equation (3),

$$U = 2\pi R^3 \left[\frac{\langle p^2 \rangle}{3\rho c^2} - \frac{\rho \langle u^2 \rangle}{2} \right]. \tag{3}$$

With this equation, it is possible to calculate the acoustic radiation force applied in a particle of radius R from the potential U. In equation (3), p represents the acoustic pressure amplitude and u represents the velocity distribution in the

fluid medium. More detailed justifications can be found in (Andrade *et al.*, 2015a). Furthermore, the use of this theory does not take into account informations related, for example, to particle density or mass to determine its behavior in the fluid. Such characteristics make straightforward - and computationally advantageous - to predict the particle behavior. In the respective color scale, red represents the regions with the highest potential and in blue those with the lowest potential.

During the simulations of the transducer working at the desired frequency of 23 kHz, there was no evidence that any type of the aluminum rupture could occur and, in addition, it was possible to observe its ability to produce a satisfactory mechanical wave. Furthermore, the simulations indicate that the set-up defined by the transducer, air, and concave reflector is capable to generate the results (pressure, node and anti-node positions and potential) coherent to those desired. As a result, the transducers were constructed (Figure 2) and then the experiments were performed which results are described below.

3. EXPERIMENTAL RESULTS AND DISCUSSIONS

3.1 Resonance frequency: experimental validation

At resonant frequency, a piezoelectric oscillator reaches maximum conductance and at the frequency of anti-resonance reaches maximum electrical resistance (Tayra, 2014). Piezoelectric ceramics can be simplified in electrical terms as an electrical component with resistance, reactance, conductance and susceptance. In the resonance frequency, the impedance is minimal due to the high conductance, and in the anti-resonance frequency the impedance is maximum due to the high resistance. As verified in the computational simulations described previously, in the resonance frequency, it can be observed greater mechanical tensions and displacements (Uchino and Giniewicz, 2003).

A practical way ot observe the resonance frequency is through the electrical impedance curve of the transducer (Tayra, 2014). The impedance *versus* the transducer frequency curve indicates the resonance frequency since a large variation in the impedance value at the resonance is expected. The electrical impedance measurement was performed with the Hewlett-Packard HP4194A impedance analyzer. It is important to note that the impedance curve depends not only on the ceramic but on the complete set-up of the transducer. For instance, modifications in the metallic masses and application of different voltages intensities could change the impedance curve, i.e., the resonance frequency.

Figure 9 shows the impedance curves *versus* frequency for the two fabricated transducers. The expected resonance value for the two transducers is 23 kHz, however, as can be observed, transducer A has a resonance frequency of 23.61 kHz with a minimum impedance of 71.46 Ω and the transducer B has, respectively, 23.35 kHz and 222.7 Ω. Comparing to the computational simulation results, transducer A has a relative error of 2.65%, and transducer B has a relative error of 1.5%. Regardless of transducer B has the smallest relative error, it is transducer A that has a lower impedance and a better defined resonance value. This indicates greater mechanical efficiency of transducer A at the resonant frequency.

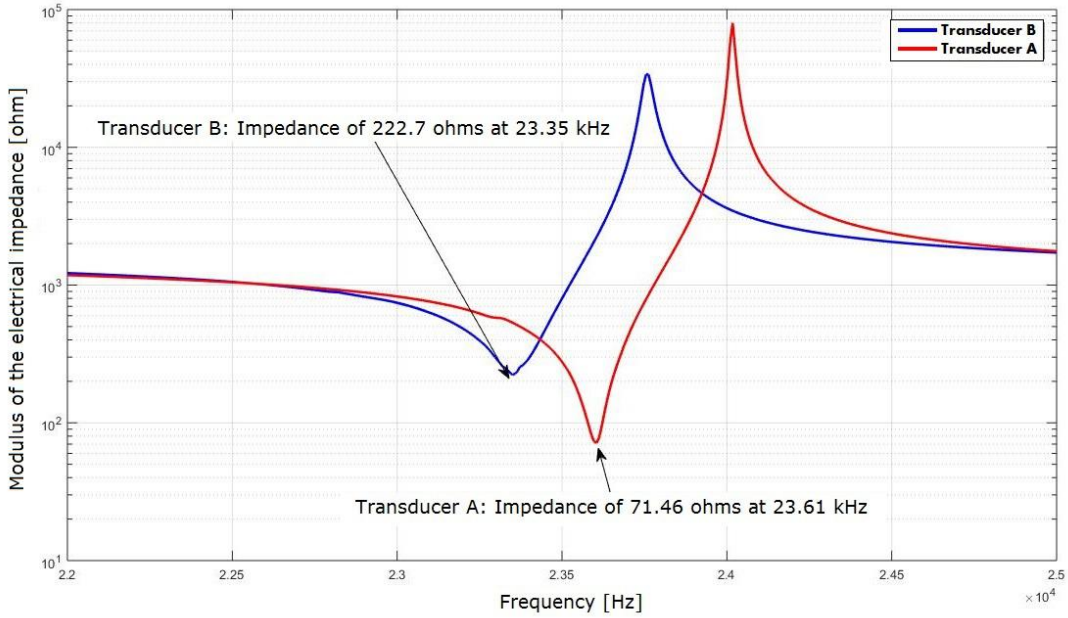

Figure 9: Impedance curves for the transducers obtained using the Hewlett-Packard HP4194A impedance analyzer.

The relative error of the experimental frequency, compared to the simulated frequency, can be caused by several factors. The first one could be related to the absence of some elements in the simulation. The small cut in the metal, the copper electrode region, the insulating material and possible construction imperfections of the aluminum were not

considered during the simulation and, furthermore, the difficulty to obtain a more accurate model. Another factor, which can be improved in a future work, is related to the insulation material manufacturing. Here, this material to not fits perfectly in the middle of the ceramic.

Finally, Figure 10 contains the equivalent electrical circuits for each transducer. These schematics were generated by the employment of the Hewlett-Packard HP4194A impedance analyzer. These equivalent circuits allow predicting the electrical impedance curves of Figure 9 and, moreover, circuits are particularly interesting due to the fact that they can be used in electrical circuit analysis environments, helping and improving the design of other components of the system (e.g., a power supply).

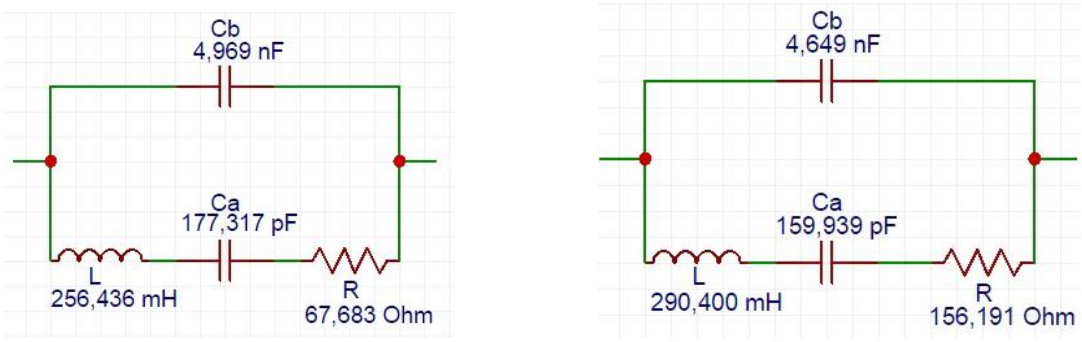

(a) Transducer A. (b) Transducer B.

Figure 10: Electric circuits constructed with basic electronic elements - resistors, capacitors and inductors - that can be used to simulate the transducers in an electrical circuit analysis environments.

3.2 Acoustic levitation

A sinusoidal signal with the desired frequency for electrical and, consequently, mechanical (via piezoelectric effect) excitations is provided by a function generator. The waveform of the function generator is amplified by a power amplifier which is connected to the transducer by a wire welded on the copper electrode. The fabricated transducers are of high power, and the piezoelectric ceramic works with typical voltages above 50 V, which provides mechanical deformations of the order of micrometers or nanometers. Although the simulation using 80 V shows tension leakage far from the rupture tension (see Figure 6), it is recommended to start the tests with a lower voltage and increase it gradually, following and observing the behavior of the transducer.

Therefore, the transducers were initially connected with 0 V and the voltage was gradually increased, using the frequency observed for each transducer in the impedance analyzer. The displacement amplitude increases linearly with the voltage amplitude also increasing the kinetic energy dissipated by the transducer, because despite the fact that increasing the displacement of the transducer face, the frequency remains the same. Near the applied voltage of 60 V, both transducers began to make an unpleasant noise in the audible range, being that in 65.25 V for transducer A and 64.35 V for transducer B. At this moment, the increase of the applied voltage was ceased due to the strong noise.

By using a height adjuster, it was possible to adjust the distance between the transducer and the concave reflector in order to obtain a multiple distance of L. With a frequency close to 23 kHz and the air-wave velocity of 345 m/s, the wavelength in the air L is about 0.015 m. The transducer was maintained at a distance of approximately 30 mm, that is, twice the wavelength value. In this case, it was expected that 4 points would be obtained for levitation of particles, as indicated in the computational simulations.

To refine the distance adjustment, a precision balance is used, as shown in Figure 11. The largest acoustic radiation force in the z-direction depends on the distance between the transducer an the reflector, and this value is precisely displayed by the balance. For the transducer A, the maximum value of the observed acoustic radiation force was 0.190 g (Figure 11(a)) and for transducer B, the value was 0.177 g (Figure 11(b)). The operation of both transducers can be seen in (Genuino and Lima, 2017).

In the levitation experiment, the two levitating particles closest to the reflector were the least stable. This is justified from the analysis of Figure 8 which demonstrates the Gor'kov potential. From there, it can be observed that the two lowest potential regions closest to the reflector do not contain a potential focus as the two closest to the transducer. By adjusting the frequency of the transducer A to operate at 23.54 kHz and the transducer B to 23.06 kHz, the particles exhibited a more attenuated oscillatory behavior. This frequency difference compared to that shown by the impedometer is due to the fact that the transducer vibration itself. For instance, the increase in temperature of the transducer during its operation, changing its physical properties.

Considering the transducer A, which showed greater stability, an additional test was performed: a water particle was inserted as shown in Figure 11(c). To levitate a larger particle, a greater pressure range obtained with a greater

(a) Transducer A.

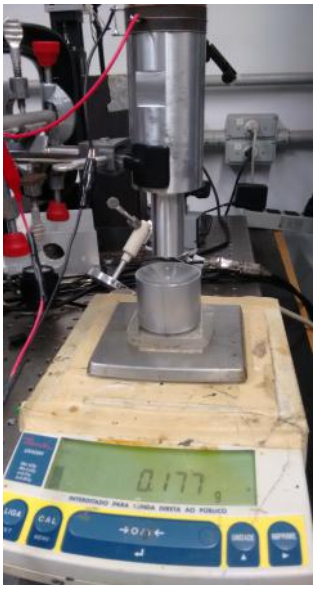

(b) Transducer B.

(c) Water drop.

Figure 11: Maximum values of the observed acoustic radiation for both transducers. In (c) one can observe a small water drop being levitated by the transducer A.

displacement of the transducer face would be required. This was not possible with the transducers built due to the high noise emitted.

Finally, it should be noted that levitation by the standing wave technique allows the levitation of bodies of size close to a quarter of the wavelength (size of the wave-to-particle pressure node equilibrates). As analyzed by Andrade *et al.* (2015a), for the levitation of larger particles, it is necessary to decrease the frequency, increasing the wavelength, which would lead to the frequency of resonance to the audible region. Usually, acoustic levitation of objects requires pressure levels on the order of 160 dB. According to the World Health Organization, for values above 140 dB, the eardrum can be damaged, so it is important to keep the ultrasound frequency above the audible frequency.

4. CONCLUSIONS

In this work, an acoustic transducer was designed to perform the levitation of small objects. The transducer was designed and simulated using the COMSOL software, which was used to tune the dimensions of the transducer. Based on the simulations, two real transducers were fabricated and the levitation of expanded polystyrene particles was experimentally demonstrated. The mechanic characteristics of the transducer were assessed, corroborating the simulation results.

5. ACKNOWLEDGEMENTS

This work was supported by CNPq (grant number 449699/2014-5). The authors would like to thank Prof. Dr. Ricardo Suyama for all the support and Prof. Dr. Carlos Alberto dos Reis Filho for the suggestions.

6. REFERENCES

Andrade, M.A.B., Bernassau, A.L. and Adamowski, J.C., 2016. "Acoustic Levitation of a Large Solid Sphere". *Applied Physics Letters*, Vol. 109, No. 4, pp. 1–5. doi:10.1063/1.4959862.

Andrade, M.A.B., Buiochi, F.C. and Adamowski, J.C., 2010. "Finite Element Analysis and Optimization of a Single-Axis Acoustic Levitator". *IEEE Transactions on Ultrasonics, Ferroelectrics, and Frequency Control*, Vol. 57, No. 2, pp. 469–479. doi:10.1109/TUFFC.2010.1427.

Andrade, M.A.B., Okina, F.T.A., Bernassau, A.L. and Adamowski, J.C., 2017. "Acoustic Levitation of an Object Larger than the Acoustic Wavelength". *The Journal of the Acoustical Society of America*, Vol. 141, No. 6, pp. 4148–4154. doi:10.1121/1.4984286.

Andrade, M.A.B., Pérez, N. and Adamowski, J.C., 2015a. "Levitação Acústica". *Revista Brasileira de Ensino Física*, Vol. 37, No. 2, p. 2304. doi:10.1590/S1806-11173721747. In portuguese.

Andrade, M.A.B., Pérez, N. and Adamowski, J.C., 2015b. "Particle manipulation by a non-resonant acoustic levitator". *Applied Physics Letters*, Vol. 106, No. 1, p. 014101. doi:10.1063/1.4905130.

Brandt, E.H., 1989. "Levitation in Physics". *Science*, Vol. 243, No. 4889, pp. 349–355. doi:

10.1126/science.243.4889.349.

Brandt, E.H., 2001. "Acoustic physics: Suspended by sound." *Nature*, Vol. 413, No. 6855, pp. 474–475. doi: 10.1038/35097192.

Bruus, H., 2012. "Acoustofluidics 7: The Acoustic Radiation Force on Small Particles". *Lab on a Chip*, Vol. 12, No. 6, pp. 1014–1021. doi:10.1039/c2lc21068a.

Foresti, D., Nabavi, M., Klingauf, M., Ferrari, A. and Poulikakos, D., 2013. "Acoustophoretic Contactless Transport and Handling of Matter in Air". *Proceedings of the National Academy of Sciences*, Vol. 110, No. 31, pp. 12549–12554. doi:10.1073/pnas.1301860110.

Gallego-Juarez, J.A., 1989. "Piezoelectric ceramics and ultrasonic transducers". *Journal of Physics E: Scientific Instruments*, Vol. 22, No. 10, pp. 804–816. doi:10.1088/0022-3735/22/10/001.

Gao, J.R., Cao, C.D. and Wei, B., 1999. "Containerless processing of materials by acoustic levitation". *Advances in Space Research*, Vol. 24, No. 10, pp. 1293–1297. doi:10.1016/S0273-1177(99)00736-X.

Genuino, I.M. and Lima, B.E.C., 2017. "Levitação Acústica". Undergraduate final project. Supplementary material. Engenharia de Instrumentação, Automação e Robótica (EIAR), Universidade Federal do ABC (UFABC). In portuguese. URL `https://www.youtube.com/watch?v=3F3CzUdLmZg`.

Grier, D.G., 2003. "A revolution in optical manipulation". *Nature*, Vol. 424, No. 6950, pp. 810–816. doi: 10.1038/nature01935.

Kaplan, B.Z., 1967. "Analysis of a method for magnetic levitation". *Proceedings of the Institution of Electrical Engineers*, Vol. 114, No. 11, pp. 1801–1804. doi:10.1049/piee.1967.0343.

Koyama, D. and Nakamura, K., 2010. "Noncontact Ultrasonic Transportation of Small Objects Over Long Distances in Air Using a Bending Vibrator and a Reflector". *IEEE Transactions on Ultrasonics, Ferroelectrics, and Frequency Control*, Vol. 57, No. 5, pp. 1152–1159. doi:10.1109/TUFFC.2010.1527.

Lima, B.E.C. and Genuino, I.M., 2017. *Desenvolvimento de um Transdutor Ultrassônico Aplicado na Levitação Acústica*. Undergraduate final project, Engenharia de Instrumentação, Automação e Robótica (EIAR), Universidade Federal do ABC (UFABC). In portuguese.

Marzo, A., Seah, S.A., Drinkwater, B.W., Sahoo, D.R., Long, B. and Subramanian, S., 2015. "Holographic acoustic elements for manipulation of levitated objects". *Nature Communications*, Vol. 6, p. 8661. doi:10.1038/ncomms9661.

Santesson, S. and Nilsson, S., 2004. "Airborne chemistry: Acoustic levitation in chemical analysis". *Analytical and Bioanalytical Chemistry*, Vol. 378, No. 7, pp. 1704–1709. doi:10.1007/s00216-003-2403-2.

Scheeline, A. and Behrens, R.L., 2012. "Potential of levitated drops to serve as microreactors for biophysical measurements". *Biophysical Chemistry*, Vol. 165–166, No. Supplement C, pp. 1–12. doi:10.1016/j.bpc.2012.03.008.

Silva, J.B., 2006. *Análise numérica de um transdutor piezelétrico de potência para processamento de termoplásticos têxteis*. Master's thesis, Universidade de São Paulo. In portuguese.

Tayra, V.T., 2014. *Desenvolvimento de um transdutor ultrassônico de potência aplicado em perfuração de rochas e usinagem de metal*. Master's thesis, Universidade de São Paulo. In portuguese.

Uchino, K. and Giniewicz, J.R., 2003. *Micromechatronics*. CRC Press.

Vandaele, V., Lambert, P. and Delchambre, A., 2005. "Non-contact handling in microassembly: Acoustical levitation". *Precision Engineering*, Vol. 29, No. 4, pp. 491–505. doi:10.1016/j.precisioneng.2005.03.003.

Xie, W.J., Cao, C.D., Lü, Y.J., Hong, Z.Y. and Wei, B., 2006. "Acoustic method for levitation of small living animals". *Applied Physics Letters*, Vol. 89, No. 21, p. 214102. doi:10.1063/1.2396893.

Xie, W.J., Cao, C.D., Lü, Y.J. and Wei, B., 2002. "Levitation of Iridium and Liquid Mercury by Ultrasound". *Physical Review Letters*, Vol. 89, No. 10, p. 104304. doi:10.1103/PhysRevLett.89.104304.

Xie, W.J. and Wei, B., 2001. "Parametric Study of Single-Axis acoustic Levitation". *Applied Physics Letters*, Vol. 79, No. 6, pp. 881–883. doi:10.1063/1.1391398.

Yarin, A.L., Pfaffenlehner, M. and Tropea, C., 1998. "On the acoustic levitation of droplets". *Journal of Fluid Mechanics*, Vol. 356, pp. 65–91. doi:10.1017/S0022112097007829.

7. RESPONSIBILITY NOTICE

The authors are the only responsible for the printed material included in this paper.